^{129}Xe NMR Spectroscopy of Metal Carbonyl Clusters and Metal Clusters in Zeolite NaY

Andrea Labouriau,*,† Ghansham Panjabi,‡ Bryan Enderle,‡ Tanja Pietrass,§ Bruce C. Gates,‡ William L. Earl,† and Kevin C. Ott†

Contribution from the Chemical Science and Technology Division, Mail Stop J514, Los Alamos National Laboratory, Los Alamos, New Mexico 87545, Department of Chemical Engineering and Materials Science, University of California, Davis, California 95616, and Department of Chemistry, New Mexico Institute of Mining and Technology, Socorro, New Mexico 87801

Received February 19, 1999

Abstract: $[Ir_4(CO)_{12}]$ and $[Ir_6(CO)_{16}]$ were synthesized in the pores of zeolite NaY by reductive carbonylation of sorbed $[Ir(CO)_2(acac)]$, and $[Rh_6(CO)_{16}]$ was similarly synthesized from $[Rh(CO)_2(acac)]$. The supported metal carbonyl clusters were decarbonylated to give supported clusters modeled on the basis of extended X-ray absorption fine structure spectra as Ir_4, Ir_6, and Rh_6, respectively. The supported metal carbonyl clusters and the supported metal clusters formed by their decarbonylation were investigated by ^{129}Xe NMR spectroscopy at temperatures in the range of 100−305 K. As the temperature increased, the chemical shift decreased. The curves representing the chemical shift as a function of temperature for xenon sorbed on the zeolite that contained clusters modeled as Ir_4, Ir_6, and Rh_6 were all essentially the same and hardly different from that observed for the bare zeolite NaY. This comparison leads to the conclusion that xenon is less strongly adsorbed on the decarbonylated metal clusters than on the zeolite framework. Larger chemical shifts were observed for the zeolites containing the metal carbonyl clusters, with the largest being observed for the zeolite containing $[Ir_4(CO)_{12}]$. These results are explained on the basis of the cluster sizes and NaY zeolite geometry. We suggest that the contact between xenon and $[Ir_4(CO)_{12}]$ cluster is better than that between xenon and $[Ir_6(CO)_{16}]$ or xenon and $[Rh_6(CO)_{16}]$ clusters because these two larger clusters almost fill the zeolite supercages and exclude xenon, whereas $[Ir_4(CO)_{12}]$ in the supercages is small enough to allow entry of the xenon.

Introduction

Metal clusters dispersed in the pores of zeolites are important industrial catalysts, exemplified by the Pt in zeolite LTL used for naphtha reforming.[1] Such materials have been investigated frequently because of their practical importance and because of the opportunities they offer for understanding the properties of extremely small isolated clusters.[2] The small sizes and uniformities of zeolite cages, exemplified by faujasites, which have supercage diameters of about 12 Å and window diameters about 7.5 Å, may limit the sizes of the encaged clusters, helping to make them more nearly uniform than the clusters of typical supported metal catalysts. Nonetheless, zeolite-supported metal clusters are typically far from uniform and—as a consequence of their nonuniformity and small sizes—less than well understood structurally. Transmission electron microscopy (TEM) and extended X-ray absorption fine structure (EXAFS) spectroscopy have been used extensively for determining cluster sizes.[2,3] However, with TEM it is difficult to distinguish the smallest clusters from the zeolite background, and with EXAFS spectroscopy, only average structural information is obtained.

Since the discoveries of Ito and Fraissard,[4] ^{129}Xe NMR spectroscopy has also been widely used for investigating zeolite-supported metals.[5−13] ^{129}Xe is a uniquely suitable probe of zeolite pores, having favorable NMR properties (with spin $I = 1/2$ and a relatively high NMR sensitivity) as well as being inert and small enough (with a diameter of 4.4 Å) to fit in the pores. The chemical shifts of ^{129}Xe are sensitive to the pore geometry and chemical surroundings and have been used in attempts to probe metal clusters in the pores.

Several obstacles make it difficult to assign a ^{129}Xe NMR chemical shift to a particular site in a metal cluster-containing zeolite: (1) the samples investigated have been structurally nonuniform, incorporating clusters and particles of various sizes and shapes and locations that are not well-known; (2) at the temperatures of almost all the reported ^{129}Xe NMR experiments,

† Los Alamos National Laboratory.
‡ University of California.
§ New Mexico Institute of Mining and Technology.

(1) *Oil Gas J.* **1992**, *190*, 29.
(2) Gates, B. C. *Chem. Rev.* **1995**, *95*, 511.
(3) Schwank, J.; Allard, L. F.; Deeba, M.; Gates, B. C. *J. Catal.* **1993**, *84*, 27.
(4) Ito, T.; Fraissard, J. In *Proceedings of the 5th International Conference on Zeolites; Naples, Italy, 1980*; Rees, L. V., Ed.; Heyden: London, 1980; p 510.
(5) De Menorval, L. C.; Fraissard, J.; Ito, T. *J. Chem. Soc., Faraday Trans. 1* **1982**, *78*, 403.
(6) Grosse, R.; Burmeister, R.; Boddenberg, B. *J. Phys. Chem.* **1991**, *95*, 2443.
(7) Ryoo, R.; Cho, S. J.; Pak, C.; Kim, J. G.; Ihm, S. K.; Lee, J. Y. *J. Am. Chem. Soc.* **1992**, *114*, 76.
(8) Boudart, M.; Ryoo, R.; Valenca, G. P.; Van Grieken, R. *Catal. Lett.* **1993**, *17*, 273.
(9) Pak, C.; Cho, S. J.; Lee, J. Y.; Ryoo, R. *J. Catal.* **1994**, *149*, 61.
(10) Moudrakovski, I. L.; Ratcliffe, C. I.; Ripmeester, J. A. *J. Am. Chem. Soc.* **1998**, *120*, 3123.
(11) Guillemot, D.; Polisset-Thfoin, M.; Fraissard, J. *J. Chem. Phys. B* **1997**, *101*, 8243.
(12) Hwang, I. C.; Woo, S. I. Zeolites and Related Microporous Materials: State of the Art. In *Stud. Surf. Sci. Catal.* **1994**, *84*, 757.
(13) Coddington, J. M.; Howe, R. F.; Yong, Y. S. *J. Chem. Soc., Faraday Trans.* **1990**, *86*, 1015.

10.1021/ja990532j CCC: $18.00
Published on Web 08/06/1999

Xe exchanges rapidly between zeolite cages and, when Xe gas is present, Xe can also exchange with the gas phase between zeolite particles, so that the chemical shift reflects an average over all these environments; and (3) there is not yet a theory to explain fully the nature of ^{129}Xe NMR chemical shifts in zeolites. Consequently, workers have relied on empirical models, usually that proposed by Ito and Fraissard.[14] A theoretical approach based on Grand Canonical Monte Carlo (GCMC) simulations was proposed by Jameson et al.,[15−19] with application to zeolite A, which has such small pore windows that exchange of Xe atoms between cages is highly constrained. More recently, Jameson and Lim[20] carried out GCMC simulations of xenon in AgA zeolite. The GCMC results for the average ^{129}Xe NMR chemical shifts and the xenon distributions are in good agreement with the experimental results reported by Moudrakovski et al.[10]

Our goal was to use ^{129}Xe NMR spectroscopy to provide more persuasive evidence of encaged metal clusters, which can be made to be nearly uniform by synthesis from organometallic precursors in zeolite Y. In the relatively open and unconstrained pore structure of zeolite Y, the fast exchange can be slowed by reduction of the temperature, which decreases the thermal energy of Xe. Consequently, we have measured ^{129}Xe NMR chemical shifts over a wide temperature range (100−305 K) for samples prepared from organometallic precursors to give nearly uniform metal carbonyl clusters in the supercages of zeolite NaY. Data are reported both for these metal carbonyl clusters and for the clusters formed by their decarbonylation under mild conditions, represented as approximately Ir_4, Ir_6, and Rh_6. The samples have been characterized by infrared and EXAFS spectroscopies as well as ^{129}Xe NMR spectroscopy.

Experimental Section

Zeolite Preparation. Zeolite NaY, $Na_xSi_{192-x}O_{384}Al_x$, having a cubic unit cell with space group *Fd*3*m* and cell parameter $a = 24.85$ Å and containing eight sodalite and eight supercages (α-cages) with centers forming a diamond lattice, was obtained from the Davison Division of W. R. Grace and Co. ^{29}Si MAS NMR was used to determine the Si/Al atomic ratio of 2.6 as calculated by the peak ratios of Si(1Al), Si(2Al), etc. Syntheses of metal clusters in the zeolites and sample transfers were performed with exclusion of air and moisture on a double-manifold Schlenk vacuum line and in a N_2-filled glovebox (AMO-2032, Vacuum Atmospheres). He, CO, and H_2 (99.995%) were purified by passage through traps containing particles of Cu and activated zeolite to remove traces of O_2 and moisture, respectively. *n*-Pentane (99.0% purity, Aldrich), used as a solvent, was refluxed under N_2 in the presence of Na/benzophenone ketyl to remove traces of water and deoxygenated by sparging of dry N_2 prior to use. $[Rh(CO)_2(acac)]$ (dicarbonylacetylacetonatorhodium (I), Strem, 99%) and $[Ir(CO)_2(acac)]$ (dicarbonylacetylacetonatoiridium (I), Strem, 99%) were used as received. The zeolite support was initially calcined at 573 K in flowing O_2 (Matheson Extra Dry Grade) for 2 h and evacuated at 10^{-3} Torr at the final calcination temperature for 14 h.

Zeolite-supported $[Ir_4(CO)_{12}]$ was prepared by slurrying the zeolite support with $[Ir(CO)_2(acac)]$ in *n*-pentane followed by room-temperature evacuation and reductive carbonylation in CO at 313 K.[21] $[Ir_6(CO)_{16}]$ was synthesized similarly, with the carbonylation at 398 K.[21] Zeolite-supported $[Rh_6(CO)_{16}]$ was prepared by slurrying the zeolite with $[Rh(CO)_2(acac)]$ in *n*-pentane followed by room-temperature evacuation and reductive carbonylation in CO at 398 K for 12 h.[23]

The samples were decarbonylated by treatment in flowing He or H_2 as the temperature was increased (3 K/min) from 25 to 573 K and then held at that temperature for 2 h, as described elsewhere.[21−23] The metal loading was 3.3 wt % for $[Ir_4(CO)_{12}]$, 3.3 wt % for $[Ir_6(CO)_{16}]$, and 2.4 wt % for $[Rh_6(CO)_{16}]$.

Infrared Spectroscopy. Spectra were recorded with a Bruker IFS-66V spectrometer with a spectral resolution of 4 cm^{-1}. Samples were pressed into self-supporting wafers and mounted in the cell in the drybox. Details are as given elsewhere.[21−23]

EXAFS Spectroscopy. EXAFS experiments were performed at X-ray beamline X-11A at the National Synchrotron Light Source (NSLS), Brookhaven National Laboratory, Upton, NY. The storage ring at BNL operated with an energy of 2.5 GeV; the ring current was 140−240 mA. The data were collected with the samples under vacuum (10^{-5} Torr) at approximately liquid nitrogen temperature. Data were collected at the Ir L_{III} and Rh K edges.[21−23]

NMR Measurements. The samples characterized by NMR were weighed and packed into 8 mm diameter glass tubes (Wilmad) in a He-filled glovebox. The zeolite NaY sample was heated for 12 h at 723 K under vacuum to remove water, then cooled to room temperature under vacuum. A known amount of Xe gas was condensed and frozen inside each glass tube. Furthermore, about 18 Torr of He was introduced into the tube to increase the rate of heat transfer during the NMR experiments. The glass tube was then flame sealed. The Xe concentration in each sample was 0.5 Xe atoms/supercage.

The ^{129}Xe NMR experiments were performed with a homemade transmission line probe on a Varian Unity 400 spectrometer operating at 110.629 MHz. The typical $\pi/2$ pulse width was 10 μs, and a 3-s recycle delay was used for the temperature range investigated. The number of transients per spectrum varied from 200 to 512, depending on the sample temperature. Low temperatures were achieved with an Oxford model CF 1200 cryostat. Temperature was measured with the Au−Fe/constantan thermocouple, which is part of the temperature-sensing and -controlling circuit in the Oxford cryostat, and with a calibrated carbon−glass resistor mounted in a copper block that is part of the probe structure. The sample was cooled in steps from room temperature to 100 K, being allowed to equilibrate for 20−30 min between temperature steps. Chemical shifts were measured at each step. Accurate chemical shift referencing was difficult in these experiments. We measured the chemical shift, at room temperature, of an external standard sample of Xe gas at 2.0 atm prior to each set of measurements at variable temperatures. The shift was then corrected to zero pressure with equations given by Jameson et al.[24,25]

EXAFS Data Analysis. The EXAFS data were analyzed with experimentally determined reference files obtained from EXAFS data characterizing materials of known structure. The parameters used to extract these results from the EXAFS data are published.[21−23] The EXAFS data were extracted from the spectra with the XDAP software.[26] The EXAFS function characterizing each sample was obtained from the X-ray absorption spectrum by a cubic spline background subtraction and normalized by dividing the absorption intensity by the height of the absorption edge. The final normalized EXAFS function characterizing each sample was obtained from the average of four scans. The main contributions to the spectra were isolated by inverse Fourier transformation of the final EXAFS function. The analysis was done with the Fourier-filtered data. The parameters characterizing both low-*Z* (O, C) and high-*Z* (Ir, Rh) contributions were determined by multiple-shell fitting in *r* space (where *r* is the distance from the absorbing atom,

(14) Ito, T.; Fraissard, J. *J. Chem. Phys.* **1982**, *76*, 5225.
(15) Jameson, C. J.; Jameson, A. K.; Gerald, R., II; de Dios, A. C. *J. Chem. Phys.* **1992**, *96*, 1676.
(16) Jameson, C. J.; Jameson, A. K.; Gerald, R., II; de Dios, A. C. *J. Chem. Phys.* **1992**, *96*, 1690.
(17) Jameson, C. J.; Jameson, A. K.; Baello, B. I.; Lim, H. M. *J. Chem. Phys.* **1994**, *100*, 5965.
(18) Jameson, C. J.; Jameson, A. K.; Gerald, R., II; Lim, H. M. *J. Chem. Phys.* **1995**, *103*, 8811.
(19) Jameson, C. J.; Jameson, A. K.; Lim, H. M. *J. Chem. Phys.* **1997**, *107*, 4364.
(20) Jameson, C. J.; Lim, H. M. *J. Chem. Phys.* **1997**, *107*, 4373.
(21) Kawi, S.; Chang, J. R.; Gates, B. C. *J. Phys. Chem.* **1993**, *97*, 10599.
(22) Kawi, S.; Chang, J. R.; Gates, B. C. *J. Am. Chem. Soc.* **1993**, *115*, 4830.
(23) Weber, W. A.; Gates, B. C. *J. Phys. Chem. B* **1997**, *101*, 10423.
(24) Jameson, A. K.; Jameson, C. J.; Gutowsky, H. S. *J. Chem. Phys.* **1970**, *53*, 2310.
(25) Jameson, C. J.; Jameson, A. K.; Cohen, S. M. *J. Chem. Phys.* **1975**, *62*, 4424.
(26) Vaarkamp, M.; Linders, J. C.; Koningsberger, D. C. *Physica B* **1995**, *209*, 159.

Table 1. EXAFS Results at the Ir L_{III} Edge Characterizing the Species Formed by Adsorption of $[Ir(CO)_2(acac)]$ in Zeolite NaY after Treatment in CO at 1 atm and 313 K for 12 h[a]

shell	N	R (Å)	$10^3\Delta\sigma^2$ (Å^2)	ΔE_0 (eV)	EXAFS ref
Ir−Ir	3.1	2.66	3.1	0.3	Pt−Pt
$Ir-O_{support}$	0.4	2.30	4.7	1.9	Pt−O
Ir−CO					
Ir−C	2.9	1.87	2.8	3.3	Ir−C
Ir−O*	3.2	2.90	5.1	7.3	Ir−O*

[a] Notation: N, coordination number; R, distance between absorber and backscatterer atoms; $\Delta\sigma^2$, Debye−Waller factor; ΔE_0, inner potential correction.

Table 2. EXAFS Results at the Ir L_{III} Edge Characterizing the Species Formed by Decarbonylation of $[Ir_4(CO)_{12}]$ in Zeolite NaY in H_2 at 573 K[a]

shell	N	R (Å)	$10^3\Delta\sigma^2$ (Å^2)	ΔE_0 (eV)	EXAFS ref
Ir−Ir	3.2	2.67	3.5	0.7	Pt−Pt
$Ir-O_{support}$					
$Ir-O_s$	1.3	2.17	1.9	−11.4	Pt−O
$Ir-O_l$	0.6	2.69	−3.1	−8.9	Pt−O

[a] Notation as in Table 1; the subscripts s and l refer to short and long, respectively.

Ir or Rh) and in k space (k is the wave vector) with application of k^1 and k^3 weighting in the Fourier transformations. The fit was optimized by use of a difference file technique[27] with phase- and amplitude-corrected Fourier transforms.[21−23]

Results

Infrared and EXAFS Evidence of $[Ir_4(CO)_{12}]$, $[Ir_6(CO)_{16}]$, and $[Rh_6(CO)_{16}]$ in Zeolite NaY. Infrared spectra of the samples prepared from $[Ir(CO)_2(acac)]$ and zeolite NaY, followed by treatment in CO at 313 K and 1 atm for 12 h or at 398 K and 1 atm for 12 h, match those reported,[21,22] indicating the formation of $[Ir_4(CO)_{12}]$ and $[Ir_6(CO)_{16}]$, respectively. The yield of $[Ir_4(CO)_{12}]$ was about 85%, as estimated from the υ_{CO} band intensities in the infrared spectra, and the sample contained 3.3 wt % Ir, corresponding to one cluster per 11 supercages. Similarly, the yield of $[Ir_6(CO)_{16}]$ was about 85% and the sample contained 3.3 wt % Ir, corresponding to one cluster per 16 supercages. The spectra are not sufficient for identification of metal carbonyls other than those mentioned; such species may be mononuclear species related to the precursors. Upon treatment of each of the samples in H_2 at 573 K, the υ_{CO} band intensities decreased continuously, becoming negligible after 2 h and indicating full decarbonylation.

Infrared spectra of the sample prepared from $[Rh(CO)_2(acac)]$ and zeolite NaY, after treatment in CO at 398 K and 1 atm for 12 h,[23] indicated the formation of $[Rh_6(CO)_{16}]$, with a yield of about 80%; the sample contained 2.4 wt % Rh, corresponding to one cluster per 12 supercages.[23] As before,[23] there was no evidence for the presence of higher-nuclearity rhodium carbonyls. Upon treatment of the sample in He at 573 K, the intensities of the υ_{CO} bands declined, becoming negligible after 2 h, indicating full decarbonylation.

Structural parameters determined from the EXAFS data characterizing the zeolite-supported sample formed from $[Ir(CO)_2(acac)]$ after treatment in CO at 313 K and 1 atm are consistent with the infrared results, indicating the formation of $[Ir_4(CO)_{12}]$. The data (Table 1) indicate a tetrahedral tetrairidium frame (Ir−Ir coordination number = 3.1, with an experimental uncertainty of ±20%) with three carbonyl ligands per Ir atom (Ir−C coordination number = 2.9 ± 50% and Ir−O* coordination number = 3.2 ± 50%; O* is the carbonyl oxygen), consistent with an earlier report.[21]

Table 3. EXAFS Results at the Ir L_{III} Edge Characterizing the Species Formed by Adsorption of $[Ir(CO)_2(acac)]$ in Zeolite NaY after Treatment in CO at 1 atm and 398 K for 12 h[a]

shell	N	R (Å)	$10^3\Delta\sigma^2$ (Å^2)	ΔE_0 (eV)	EXAFS ref
Ir−Ir	4.1	2.76	1.5	1.9	Pt−Pt
Ir−CO					
$Ir-C_b$	1.9	2.22	1.7	1.6	Ir−C
$Ir-C_t$	2.0	1.89	2.9	−3.4	Ir−C
Ir−O*	3.6	3.01	3.6	−7.3	Ir−O*

[a] Notation as in Table 1; the subscripts b and t refer to bridging and terminal, respectively; O* is the carbonyl oxygen.

Table 4. EXAFS Results at the Rh K Edge Characterizing the Species Formed by Adsorption of $[Rh(CO)_2(acac)]$ in Zeolite NaY after Treatment in CO at 1 atm and 398 K for 12 h[a]

shell	N	R (Å)	$10^3\Delta\sigma^2$ (Å^2)	ΔE_0 (eV)	EXAFS ref
Rh−Rh	4.1	2.73	0.3	3.8	Rh−Rh
Rh−Rh (2nd)	0.8	3.89	3.4	3.8	Rh−Rh
Rh−CO					
$Rh-C_b$	1.8	2.19	−0.2	−15.5	Ru−C
$Rh-C_t$	2.5	1.86	3.5	0.7	Ru−C
Rh−O*	3.5	2.97	1.3	1.75	Ru−O*

[a] Notation as in Table 3.

Table 5. EXAFS Results at the Ir L_{III} Edge Characterizing the Species Formed by Decarbonylation of $[Ir_6(CO)_{16}]$ in Zeolite NaY in H_2 at 573 K[a]

shell	N	R (Å)	$10^3\Delta\sigma^2$ (Å^2)	ΔE_0 (eV)	EXAFS ref
Ir−Ir	4.0	2.70	3.5	−2.0	Pt−Pt
$Ir-O_{support}$					
$Ir-O_s$	0.5	2.18	7.0	−6.3	Pt−O
$Ir-O_l$	1.3	2.70	3.6	−8.2	Pt−O

[a] Notation as in Table 2.

The EXAFS data, consistent with the infrared data, show that treatment of the sample in H_2 at 573 K for 2 h led to complete cluster decarbonylation.[21] The Ir−Ir coordination number of 3.2 ± 20% is consistent with the formation of Ir_4 in the zeolite (Table 2). Since there was a negligible change in the first-shell Ir−Ir coordination number as a result of decarbonylation, the yield of Ir_4 is inferred to be approximately the same as that of $[Ir_4(CO)_{12}]$, i.e., about 85%. The uncertainty in this estimate is substantially greater than that in the estimate for $[Ir_4(CO)_{12}]$.

Similarly, EXAFS structural parameters characterizing the zeolite-supported samples made from $[Ir(CO)_2(acac)]$ and $[Rh(CO)_2(acac)]$ after treatment in CO at 398 K and 1 atm are consistent with the infrared spectra and the formation of $[Ir_6(CO)_{16}]$ (Table 3) and $[Rh_6(CO)_{16}]$ (Table 4), respectively. The data indicate hexanuclear metal frames, each with two bridging carbonyls (M−C_b, M = Ir, Rh), two terminal carbonyls (M−C_t, M = Ir, Rh), and a metal−oxygen contribution (M−O*, M = Ir, Rh). The data characterizing the rhodium carbonyl species give evidence of a second-shell Rh−Rh contribution, with a coordination number of 0.8. The data characterizing the iridium-containing sample do not give evidence of a higher-shell Ir−Ir contribution, but this result is not surprising, as only data of unusually high quality would give such evidence for a cluster with an M_6 frame. These EXAFS parameters are consistent with the formation of $[Ir_6(CO)_{16}]$[22] and $[Rh_6(CO)_{16}]$[23] in the respective samples.

Upon treatment of the zeolite-supported $[Ir_6(CO)_{16}]$ in H_2 at 573 K for 2 h, the metal frame was essentially unchanged, and there were no residual carbonyl contributions, as shown by the EXAFS data (Table 5). Correspondingly, there were increased

(27) Kirlin, P. S.; van Zon, F. B. M.; Koningsberger, D. C.; Gates, B. C. *J. Phys. Chem.* **1990**, *94*, 8439.

Table 6. EXAFS Results at the Rh K Edge Characterizing the Species Formed by Decarbonylation of $[Rh_6(CO)_{16}]$ in Zeolite NaY in He at 573 K[a]

shell	N	R (Å)	$10^3\Delta\sigma^2$ (Å^2)	ΔE_0 (eV)	EXAFS ref
Rh−Rh	3.9	2.68	3.9	4.4	Rh−Rh
Rh−$O_{support}$					
Rh−O_s	1.1	2.17	7.3	−10.0	Rh−O
Rh−O_l	1.9	2.70	2.1	−5.3	Rh−O

[a] Notation as in Table 2.

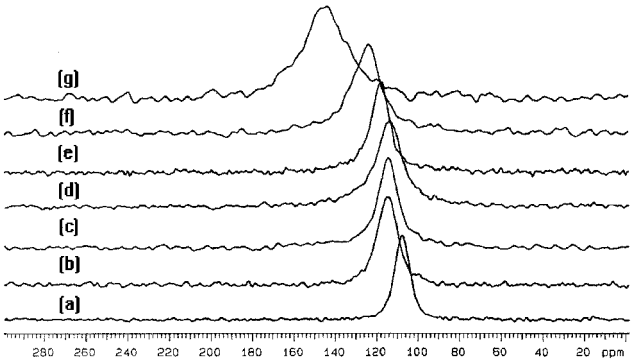

Figure 1. ^{129}Xe NMR spectra characterizing zeolite NaY (a) and zeolite NaY incorporating clusters modeled as (b) Rh_6, (c) Ir_6, (d) Ir_4, (e) $[Rh_6(CO)_{16}]$, (f) $[Ir_6(CO)_{16}]$, and (g) $[Ir_4(CO)_{12}]$ measured at 100 K.

contributions from the oxygen atoms of the support (Ir−O_s and Ir−O_l, where the subscripts s and l refer to short and long, respectively), as expected.[22]

Treatment of the supported $[Rh_6(CO)_{16}]$ in He at 573 K for 2 h led to a similar result, indicating the retention of the hexanuclear metal frame and an increased interaction of the clusters with the support (Table 6).

These results match those reported[22,23] and indicate that the clusters can be well approximated as zeolite-supported Ir_6 and Rh_6, respectively. The yields of the metal clusters, estimated as stated above, are about 85% for Ir_6 and about 80% for Rh_6.

In summary, the infrared and EXAFS results indicate the synthesis of $[Ir_6(CO)_{16}]$, $[Ir_4(CO)_{12}]$, and $[Rh_6(CO)_{16}]$ in the zeolite and the decarbonylation of each to give clusters modeled as Ir_4, Ir_6, and Rh_6, respectively. The yields range from about 80 to 85%. Although the uniformity of the clusters is less than precisely defined, they appear to be the most nearly uniform supported clusters available and thus good candidates for investigation by ^{129}Xe NMR spectroscopy.

^{129}Xe NMR Data. Figure 1 shows the ^{129}Xe NMR spectra representing xenon sorbed on bare zeolite NaY and on this zeolite containing each of the metal carbonyl and metal clusters mentioned in the preceding paragraphs. Only a single resonance signal was observed for each sample, regardless of the temperature. No NMR signal corresponding to bulk Xe gas was detected.

Chemical shifts as a function of temperature are shown in Figure 2. As reported for numerous zeolites,[28,29] the chemical shift increases as the temperature decreases. The results show that the ^{129}Xe chemical shifts are approximately the same for bare zeolite NaY and for the zeolites containing each of the decarbonylated clusters; at each temperature, these latter chemical shifts are only about 6 ppm greater than that of zeolite NaY.

The chemical shifts of Xe in the zeolites containing the metal carbonyl clusters at any of the temperatures are greater than those characterizing the zeolites containing the decarbonylated clusters (Figure 2). The values differ from one metal carbonyl cluster to another, being greatest for the $[Ir_4(CO)_{12}]$-containing sample. The results characterizing the zeolites incorporating $[Ir_6(CO)_{16}]$ and $[Rh_6(CO)_{16}]$ are not much different from each other.

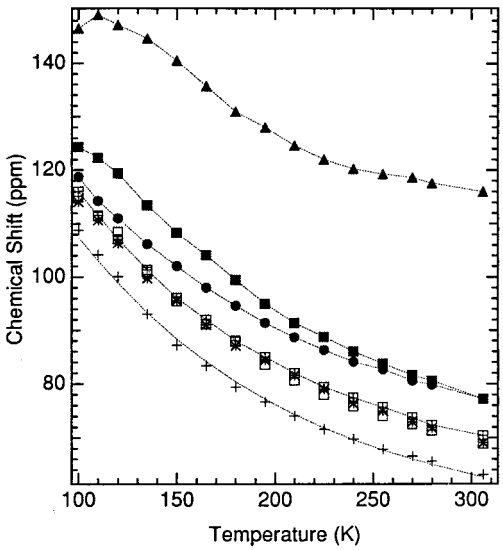

Figure 2. ^{129}Xe NMR chemical shifts at temperatures ranging from 100 to 305 K for xenon sorbed in (+) zeolite NaY and zeolite NaY containing clusters modeled as (▲) $[Ir_4(CO)_{12}]$, (■) $[Ir_6(CO)_{16}]$, (●) $[Rh_6(CO)_{16}]$, (∗) Ir_4, (□) Ir_6, and (⊞) Rh_6.

Discussion

The ^{129}Xe NMR chemical shifts reported here demonstrate for the first time differences between the shifts indicative of a bare zeolite, the zeolite containing small metal clusters of nearly uniform size and varied composition, and the zeolite containing small metal carbonyl clusters of varied size and composition. Our results are similar to those obtained by Hwang and Woo[12] as well as those reported by Coddington et al.[13] For instance, Hwang and Woo[1] performed ^{129}Xe NMR experiments to investigate a Ir/NaY sample (4 wt % Ir) synthesized by ion exchange of $Ir(NH_3)_5Cl^{2+}$ into NaY zeolite followed by calcination in O_2 and subsequent reduction in H_2. Their ^{129}Xe NMR experiments were performed at room temperature and as a function of the xenon loading. They observed a small increase of the chemical shift as the xenon pressure decreases. Coddington and co-workers[13] synthesized small molybdenum clusters in zeolite Y by adsorption of $[Mo(CO)_6]$, with an average loading of two Mo atoms per supercage. The ^{129}Xe NMR experiments were performed at room temperature and for a loading of 0.8 xenon atoms/supercage. Their results indicate a 22 ppm increase in chemical shift relative to that of zeolite NaY at the same xenon loading. This small increase in the chemical shift compared with that representing the bare zeolite is comparable to our results.

However, our data are markedly different from those reported in Table 7, which were obtained by Ryoo et al.[7] at room temperature and in the limit of zero xenon coverage for Pt, Ru, Pd, Rh, and Ir clusters or particles supported on zeolite Y. Their samples were prepared as typical zeolite-supported metal catalysts by activating zeolite samples made by ion exchange with metal ammine complexes followed by calcination in O_2 and ensuing reduction with H_2 (giving nonuniform samples containing 2.1−10 wt % metal). ^{129}Xe NMR chemical shifts were described by a model similar to the one proposed by Fraissard's group.[11,14] These shifts are markedly larger than those observed in our work.

(28) Chen, Q. J.; Fraissard, J. *J. Phys. Chem.* **1992**, *96*, 1809.
(29) Cheung, T. T. P. *J. Phys. Chem.* **1995**, *99*, 7089.

Table 7. ^{129}XeNMR Chemical Shifts Characterizing Zeolite NaY-Supported Metal Clusters, Obtained at Room Temperature and by Extrapolation to Zero Xenon Coverage[7]

metal in clusters or particles	approx av cluster or particle diameter (nm)	chemical shift, δ (ppm)
Ru	>1	950 ± 50
Ru	<1	550 ± 50
Rh	>1	3200 ± 400
Ir	>1	800 ± 50
Pd	>1	3000 ± 200
Pt	>1	1300 ± 50

In our case, we have not obtained the chemical shift in the limit of zero loading but instead at constant xenon coverage, i.e., 0.5 Xe atoms per supercage. At this low xenon loading, the contributions to the chemical shift from two Xe atoms in the same supercage are small. Molecular modeling calculations[30−32] show that most xenon atoms exist as monomers when xenon is present in zeolite NaY at low loadings. Consequently, Xe−Xe interactions are inferred to be negligible for the xenon concentration considered in the present work, although they might become more significant at low temperatures. According to results by Ratcliffe and Ripmeester,[33] xenon is mobile at temperatures as low as 77 K. Xenon adsorbed at an anisotropic site should have a chemical shift anisotropy (csa), although it might be small and then concealed by broadening from other interactions. ^{129}Xe NMR spectra of xenon at 100 K show just a broad line, with no detectable chemical shift anisotropy (Figure 1). Thus, the picture that we have of the state of xenon at 100 K is that it probably is mobile and closely associated with the inner surfaces of the zeolite framework, especially the strong adsorption sites. If we suppose that the metal clusters are stronger adsorption sites than the zeolite framework sites, then we would expect that the former would be the favorable adsorption sites at low temperatures and that the chemical shift should reflect mainly xenon sorbed on the metal clusters. However, even at 100 K, we have not detected for any of the samples investigated here any large effect of the metal cluster on the chemical shift, such as those listed in Table 7.

Thus, to interpret our data, it is helpful to recall the primary origin of xenon chemical shifts. The NMR chemical shift depends on the chemical environment of the nucleus. Hence, the chemical shift occurs when the electron cloud of an atom is distorted by an external electric field generated by the instantaneous electric dipole moments of other atoms. For example, although xenon has no permanent electric dipole moment, van der Waals interactions between xenon atoms and the zeolite framework and any adsorbed species give rise to a ^{129}Xe NMR chemical shift. The stronger the interaction between a xenon atom and a sorption site, the longer xenon resides at that site. The stronger interactions result in a larger xenon electron cloud deformation, which gives rise to an increase of the ^{129}Xe NMR chemical shift.

As long as the overlap between two interacting atoms is negligible, the chemical shift associated with the two atoms can be described by the Drude model. According to this model, the intermolecular shielding $\sigma(r)$ is a function of the London attraction energy $W(r)$ for the system.[34,35] Then, the shielding change on atom 1, relative to that of the isolated atom 1, caused by the interaction with atom 2 at a distance r is given by

$$\sigma(r) - \sigma(\infty) \approx [B/\alpha_1]W(r) \quad (1)$$

where α_1 is the xenon static electric dipole polarizability and B the shielding hyperpolarizability of xenon. $W(r)$ is the interaction energy given by the London equation:

$$W(r) = -\frac{3\alpha_1\alpha_2}{2r^6}\left[\frac{U_1U_2}{U_1 + U_2}\right] \quad (2)$$

where α_2 is the static electric dipole polarizability of atom 2 and U_1 and U_2 are the ionization potentials of atoms 1 and 2, respectively. The xenon−zeolite interaction is then modeled in terms of two short-range interactions: xenon−oxygen and xenon−sodium. It is common to neglect the interaction between xenon and the zeolite T atoms (Si and Al), because they are well shielded from xenon by the oxygen atoms.

Table 8. Physical Properties of Some Transition Metal Atoms[36]

atom	static electric dipole polarizability (Å^{-3})	ionization potential (eV)
Ru	9.6	10.75
Rh	8.6	7.46
Ir	7.6	9.1
Pd	4.8	8.34
Pt	6.5	9.0

In addition, the xenon−metal cluster interaction also needs to be accounted for. Table 8 is a list of the static electric dipole polarizabilities and ionization potentials[36] of the transition metal atoms considered here; the tabulated physical properties do not vary much from one of these atoms to another. This comparison indicates the likelihood that the interaction between a xenon atom and an isolated transition metal atom, whether it be Rh, Ir, Ru, Pd, or Pt, is approximately the same.

However, in attempting to apply similar calculations to represent a metal cluster supported in a zeolite, we encounter complications: the static electric dipole polarizability as well as the ionization potential vary as isolated atoms are combined into a cluster. Furthermore, the clusters are not bare and isolated, but interact with the zeolite walls. To our knowledge, there is no reported experimental or theoretical work regarding static electric dipole polarizabilties and ionization potentials of even bare rhodium or iridium clusters.

Nevertheless, these parameters have been extensively investigated for bare alkali metal clusters[37,38] and for silver cations and anions.[39] To a first approximation, the static electric dipole polarizability and the ionization potential of simple metal clusters can be described by the jellium model. The static electric dipole polarizability of small clusters is strongly enhanced with respect to the classical value for a conducting sphere.[37] In the jellium model, this fact is represented by writing $\alpha = (R_c + \delta R_c)^3$, where R_c is the jellium background sphere radius and

(30) Woods, G. B.; Panagiotopoulos, A. Z.; Rowlinson, J. S. *Mol. Phys.* **1988**, *63*, 49.
(31) Woods, G. B.; Rowlinson, J. S. *J. Chem. Soc., Faraday Trans. 2* **1989**, *85*, 765.
(32) Santikary, P.; Yashonath, S.; Ananthakrishna, G. *J. Phys. Chem.* **1992**, *96*, 10469.
(33) Ratcliffe, C. I.; Ripmeester, J. A. *J. Am. Chem. Soc.* **1995**, *117*, 1445.
(34) Eisenschitz, R.; London, F. *Z. Phys.* **1930**, *60*, 491.
(35) London, F. *Z. Phys. Chem. B* **1930**, *11*, 222. London, F. *Trans. Faraday Soc.* **1937**, *33*, 8.
(36) Miller, T. M. *CRC Handbook of Chemistry and Physics*, 72nd ed.; CRC Press: Boca Raton, 1992; pp 10-194 to 10-210.
(37) Knight, W. D.; Clemenger, K.; de Heer, W. A.; Saunders, W. A. *Phys. Rev. B* **1985**, *31*, 2539.
(38) Bonin, K. D.; Kadar-Kallen, M. A. *Int. J. Mod. Phys. B8* **1994**, *24*, 3313 and references therein.
(39) Fedrigo, S.; Harbich, W.; Belyaev, J.; Buttet, J. *Chem. Phys. Lett.* **1993**, *211*, 166.

δR_c is the enhancement factor, which represents the effective "spill out" of the electric charge density beyond the physical surface of the metal cluster. Thus, the effective cluster radius is larger than the radius of a spherical cluster with N atoms and the bulk solid density. For example, experimental values of the static polarizability *per atom* for sodium clusters vary from ca. 21.3 to 16.6 Å^3 for clusters containing 5 and 15 atoms,[37] respectively, whereas in the bulk limit the static polarizability per sodium atom is ca. 9.5 Å^3.

Furthermore, when calculating the xenon−metal cluster interaction, one has to take into consideration the static polarizability of the cluster as a whole. Suppose a cluster consists of N atoms; then the total static polarizability is a factor of N times greater than the static polarizability per atom. As for the metal cluster ionization potential, a trend in which the potential varies inversely with the cluster radius is usually observed. For example, measured ionization potentials of sodium clusters decrease from 4.9 to 4.0 eV as the number of atoms per cluster increases from 2 to 8.[40] Also, the coefficient of the $1/r$ term depends on the metal and on the range of cluster sizes.[41]

On the basis of the above discussion, one would expect that the ^{129}Xe NMR chemical shift would have a strong dependence on the cluster size, becoming larger as the cluster size increases. However, at room temperature the mobility of xenon in zeolite NaY is such that only one signal is observed, which represents an average of all xenon atom−surface interactions. In this fast-exchange regime, part of the ^{129}Xe NMR chemical shift is due to the different polarizabilities of the adsorption sites, but it is also affected by changes in the excluded volume within the supercage. A larger cluster leaves less free volume in the supercage; thus, the xenon−xenon interaction becomes more important since the average xenon−xenon distance within the supercage becomes shorter. Both of these effects contribute to the nature of the averaging over the various positions of xenon in the supercage, leading to changes in the average xenon chemical shift.

Furthermore, on the basis of the well-known crystal structures of the metal carbonyl precursors from which the decarbonylated clusters were formed, we estimate that Ir_4 has a diameter of about 2.7 Å and Ir_6 and Rh_6 have diameters of about 3.9 Å. Thus, these clusters are too large to fit into the sodalite cages (window aperture = 2.2 Å), but they fit easily in the supercages (which have diameters of about 12 Å), where we infer they are located. Consequently, xenon would have easy access to these small metal clusters.

On the basis of the foregoing discussion, we now assess the experimental results in two parts, the first concerning the data obtained at room temperature and the second the data obtained at low temperatures.

Chemical Shifts at Room Temperature. The chemical shifts observed for xenon sorbed in the zeolite containing clusters modeled as Ir_4, Ir_6, and Rh_6 are all essentially the same and scarcely different from that observed for xenon in the bare zeolite (Figure 2). These results can be understood if one considers the low iridium and rhodium cluster concentrations in these samples (approximately 1 Rh_6 cluster/12 supercages, 1 Ir_4 cluster/11 supercages, and 1 Ir_6 cluster/16 supercages). These low metal cluster loadings (which are greater than those of typical industrial supported metal catalysts) correspond to only little difference between the average excluded volume (or the average xenon atom−surface interactions) of the bare zeolite and the zeolite containing the metal clusters. Since xenon is highly mobile at room temperature, the small fraction of the supercages containing clusters contributes little to the average chemical shift (+6 ppm). The results broadly agree with those of Coddington et al.,[13] whose samples had a much higher metal loading (1 cluster per supercage) and thus a higher chemical shift relative to that of the bare zeolite (22 ppm).

In contrast, the metal carbonyl clusters in the zeolite exert a more significant influence on the xenon chemical shift. The chemical shifts representing xenon sorbed in the zeolites containing $[Ir_6(CO)_{16}]$ and $[Rh_6(CO)_{16}]$ at room temperature are essentially the same, 77 ppm. As these two metal clusters were present in comparable concentrations in the zeolite, and in view of the discussion above, this result can be reasoned out if we realize that these two metal clusters have approximately the same size (about 12 Å) and thus similar polarizabilities. Compared with that characterizing the decarbonylated clusters, the higher chemical shift is suggested to result from a greater polarizability associated with a larger cluster size. Another possibility is associated with the interaction between the metal carbonyl clusters and the zeolite walls. The ν_{CO} region of the infrared spectrum shows a shift of both the terminal and bridging carbonyl bands to higher frequencies relative to those of the metal carbonyls in solution.[21−23] This comparison is indicative of electron withdrawal from the metal cluster to the zeolite framework through the soft CO ligands. In this case, one would expect to observe distinct ^{129}Xe NMR chemical shifts for metal carbonyl clusters and decarbonylated clusters, since the net charge associated with these clusters is most likely to be different.

A striking result emerges from the data representing the zeolite containing $[Ir_4(CO)_{12}]$: the ^{129}Xe NMR chemical shift is ca. 116 ppm, markedly larger than that observed for the zeolite containing either of the other two metal carbonyl clusters. The $[Ir_4(CO)_{12}]$ loading is the same as the $[Ir_6(CO)_{16}]$ loading (3.3 wt %). Since the $[Ir_4(CO)_{12}]$ clusters are smaller than the hexanuclear metal carbonyls in the crystalline state[21] (9 versus 12 Å diameter), then the former clusters would occupy less volume in the zeolite than the hexanuclear clusters, which implies more free volume in the supercages in the former case. Also, because of its smaller size, $[Ir_4(CO)_{12}]$ would have a smaller polarizability, leading to smaller chemical shifts instead of larger ones. This result is discussed further below.

Chemical Shifts at Low Temperatures. As the temperature decreases, the ^{129}Xe NMR chemical shift increases for each sample investigated here. This effect arises because the probability of finding xenon at shorter distances from strong adsorption sites increases as the temperature decreases. Thus, at low temperatures xenon exchange slows down and strong adsorption sites are favored over weak ones. In zeolite NaY, the lowest-energy positions are close to the walls, which correspond to higher shifts than positions far from the walls. Furthermore, the chemical shift curves as a function of temperature show only little difference from sample to sample; they are almost identical for xenon sorbed in the bare zeolite and the zeolites containing Ir_4, Ir_6, and Rh_6 (Figure 2).

The small differences between the chemical shifts observed for the zeolites containing Ir_4, Ir_6, and Rh_6 can be understood if one assumes that the iridium and rhodium clusters are approximately the same size and that their polarizabilities are of the same order of magnitude. We infer that the lack of a significant effect of the metal cluster on the chemical shift at low temperatures is due to xenon being less strongly adsorbed on the decarbonylated metal clusters than on the bare zeolite.

(40) Robbins, E. J.; Leckenby, R. E.; Willis, P. *Adv. Phys.* **1967**, *16*, 739.

(41) Knight, W. D. *Z. Phys. D* **1989**, *12*, 315.

In other words, the potential wells associated with zeolite framework sites are deeper than those associated with the decarbonylated metal clusters.

The largest difference in chemical shifts was observed for the zeolite containing $[Ir_4(CO)_{12}]$ (Figure 2). The magnitude of the slope of the curve for this sample is also less than those representing the other samples. Furthermore, there is an increase in line width for the $[Ir_4(CO)_{12}]$ sample, as shown in Figure 1. We assume that the additional broadening observed for this resonance line is related to xenon's interacting more strongly with $[Ir_4(CO)_{12}]$ than with any of the other clusters considered here. The stronger the interaction between xenon and an adsorption site, the longer xenon would reside on that site, causing an increase of the line width. Consequently, we infer that the interaction between xenon and $[Ir_4(CO)_{12}]$ is stronger than that associated with xenon and the zeolite framework.

In contrast to the chemical shifts characterizing the zeolite containing $[Ir_4(CO)_{12}]$, those characterizing the zeolites containing $[Ir_6(CO)_{16}]$ and $[Rh_6(CO)_{16}]$ do not show much difference from the values characterizing the zeolites containing decarbonylated clusters; the chemical shift characterizing the zeolite containing $[Ir_4(CO)_{12}]$ is markedly greater. On the basis of the cluster sizes only, one would expect a higher polarizability for $[Ir_6(CO)_{16}]$ than for $[Ir_4(CO)_{12}]$, and then a higher ^{129}Xe NMR chemical shift; thus, some explanation other than the cluster size alone must be invoked.

We offer the following suggestion based on the cluster and zeolite geometries: $[Ir_6(CO)_{16}]$ and $[Rh_6(CO)_{16}]$ have diameters of about 12 Å, close to the diameter of the supercage, whereas $[Ir_4(CO)_{12}]$ has a diameter of only about 9 Å. Thus, we propose that the chances for contact between a xenon atom and a metal cluster are better for the latter cluster than for the former ones, leading to a larger chemical shift, because we infer that xenon atoms were virtually excluded from supercages containing $[Ir_6(CO)_{16}]$ and $[Rh_6(CO)_{16}]$ but that they intruded significantly into supercages containing $[Ir_4(CO)_{12}]$, where they underwent strong interactions with these soft, polarizable clusters, perhaps being retained for some time in the crowded cages. Consistent with this explanation and the small differences in chemical shifts observed for the bare zeolite and that containing $[Ir_6(CO)_{16}]$ or $[Rh_6(CO)_{16}]$, we infer that the xenon interacted with the latter two clusters only at supercage windows.

Comparison with Literature Data. At a first glance, our results appear to contradict some of those reported earlier.[5−11] However, the metal clusters in our samples are relatively well defined, nearly uniform, and very small, whereas the zeolite-supported metal clusters and particles prepared by conventional methods are usually larger and generally nonuniform. Also, the large chemical shifts reported earlier were obtained by extrapolating the data to zero xenon pressure, whereas in our samples the xenon concentration was fixed (0.5 Xe atoms/supercage). Nevertheless, by decreasing the temperature one should be able to probe the strong adsorption sites. Thus, our data lead to the conclusion that xenon-decarbonylated cluster interactions are weaker than xenon−zeolite framework interactions. Consequently, we infer that large reported ^{129}Xe NMR chemical shifts result from xenon adsorbed in zeolite Y containing relatively large and nonuniform metal clusters and particles.

The origin of the large reported ^{129}Xe NMR shifts characterizing zeolite-supported metals is far from well understood, although the Knight shift may play an important role. For instance, it is well-known that the interaction of a nuclear spin with conduction electrons through the hyperfine coupling gives rise to the Knight shift. In bulk metals, the static part of the hyperfine coupling gives rise to the Knight shift, whereas the dynamic part gives rise to the Korringa relation ($T_1 \approx T^{-1}$). Van der Klink[42] investigated small platinum particles on mineral supports by using solid-state ^{195}Pt NMR, and his results show the occurrence of a Korringa-like nuclear spin−lattice relaxation. Thus, this effect is an indication that the level spacing near the Fermi energy level is small for platinum cluster or particle sizes ranging in diameter from 10 to 30 Å. Also, there is experimental evidence[43] showing the same effect on the ^{129}Xe NMR of platinum particles in zeolite NaY. Furthermore, Rao et al.[44] investigated small rhodium clusters in zeolite NaY produced by oxidation and subsequent reduction of $[Rh_6(CO)_{16}]$ in the zeolite. They found that both the magnitude and temperature dependence of ^{1}H NMR shifts for hydrogen adsorbed on rhodium clusters differed considerably from those observed for hydrogen adsorbed on rhodium particles produced by incipient wetness impregnation of NaY zeolite with an aqueous solution of $RhCl_3$, followed by reduction with H_2. First, the shift of the hydrogen adsorbed on rhodium clusters was much larger than that of hydrogen adsorbed on catalysts with rhodium particles larger than 2 nm. The authors inferred that such effects result from the paramagnetic character of their rhodium clusters. Second, the temperature dependence of the ^{1}H NMR shift of hydrogen adsorbed on the rhodium particles on zeolite NaY was nearly constant, which is consistent with a Knight shift interpretation.[45] Consequently, the Knight shift might be significant for samples containing large metal clusters or particles, but it is probably less significant for smaller clusters such as those investigated in this work. Furthermore, it is unknown how the electronic properties of very small metal clusters are affected by the interaction with the zeolite framework.

One of the conclusions of this work is that the possibility of using ^{129}Xe NMR spectroscopy as a probe for determining the average number of atoms per metal cluster is yet to be realized. We believe that a deeper understanding of ^{129}Xe NMR chemical shifts is needed to attain such a goal.

Conclusions

$[Ir_4(CO)_{12}]$, $[Ir_6(CO)_{16}]$, and $[Rh_6(CO)_{16}]$ were synthesized in the pores of zeolite NaY by reductive carbonylation of sorbed $[Ir(CO)_2(acac)]$ and $[Rh(CO)_2(acac)]$, and each was decarbonylated to give supported clusters modeled as Ir_4, Ir_6, and Rh_6, respectively. The ^{129}Xe NMR chemical shifts characterizing xenon sorbed on the zeolite containing the clusters modeled as Ir_4, Ir_6, and Rh_6 were all essentially the same and only slightly greater than those observed for the bare zeolite at temperatures from 100 to 305 K. The interactions of xenon with the larger metal carbonyl clusters, $[Ir_6(CO)_{16}]$ and $[Rh_6(CO)_{16}]$, were also small; the largest chemical shifts were observed for the zeolite containing $[Ir_4(CO)_{12}]$. The data indicate that the interactions of xenon and decarbonylated metal clusters contributed only little to the observed chemical shifts. The small chemical shifts observed for xenon interacting with $[Ir_6(CO)_{16}]$ (or $[Rh_6(CO)_{16}]$) suggest that the interactions were only at the supercage windows, consistent with filling of the supercages by these clusters. In contrast, the larger chemical shifts observed with the smaller $[Ir_4(CO)_{12}]$ in the zeolite cages imply that the interactions of

(42) Van der Klink, J. J. *Z. Phys. D* **1989**, *12*, 327.
(43) Bifone, A.; Pietrass, T.; Kritzenberger, J.; Pines, A.; Chmelka, B. F. *Phys. Rev. Lett.* **1995**, *74*, 3277.
(44) Rao, L. F.; Pruski, M.; King, T. S. *J. Phys. Chem. B* **1997**, *101*, 5717.
(45) Slichter, C. P. *Principles of Magnetic Resonance*, 3rd ed.; Slichter, C. P., Ed.; Springer-Verlag: New York, 1990; Chapter 4.

xenon with these clusters in the zeolite supercages were strong and influenced by the cluster and zeolite geometry, as a cluster and a single xenon atom barely fit together in a supercage.

Acknowledgment. This research was supported by Los Alamos National Laboratory, U.S. Department of Energy contract No. W-7405-ENG-36 as part of the Los Alamos Catalysis Initiative. We acknowledge the support of the U.S. Department of Energy, Division of Materials Sciences, under contract No. DE-FG05-89ER45384, for its role in the operation and development of beam line X-11A at the National Synchrotron Light Source (NSLS). The NSLS is supported by the Department of Energy, Division of Materials Sciences and Division of Chemical Sciences, under contract No. DE-AC02-76CH00016. The EXAFS data were analyzed with the XDAP software.[26]

JA990532J